

NUMERICAL SIMULATION OF DIFFUSIVE AND AGGREGATION PHENOMENA IN NONLINEAR CONTINUITY EQUATIONS BY EVOLVING DIFFEOMORPHISMS

J. A. CARRILLO* AND J. S. MOLL†

Abstract. We propose a numerical algorithm for solving nonlinear continuity equations written in Lagrangian coordinates. This transformation is intimately related to variational approaches for the well-posedness of gradient flows of energy functionals with respect to the quadratic transportation distance in optimal transport theory. These schemes allow the numerical approximation of both diffusive and aggregation regimes of different models. Positivity, energy decreasing and mesh adaptation are built-in in the numerical scheme and thus, we are capable of capturing blow-up densities and of dealing with vacuum regions and merging of mass patches in a natural way.

Key words. Lagrangian coordinates, variational schemes, optimal transport, adaptive mesh, diffusion, aggregation.

AMS subject classifications. 65M99, 35K55

1. Introduction. This work is devoted to propose an alternative numerical method to solve nonlinear continuity equations of the form:

$$\frac{\partial \rho}{\partial t} = -\nabla \cdot (\rho u) := \nabla \cdot [\rho \nabla (U'(\rho) + V + W * \rho)], \quad (1.1)$$

where the unknown $\rho(t, \cdot)$ is a time-dependent probability density on \mathbb{R}^d ($d \geq 1$), $U : \mathbb{R}^+ \rightarrow \mathbb{R}$ is a density of internal energy, $V : \mathbb{R}^d \rightarrow \mathbb{R}$ is a confinement potential and $W : \mathbb{R}^d \rightarrow \mathbb{R}$ is an interaction potential. The symbol ∇ denotes the gradient operator and will always be applied to functions, while $\nabla \cdot$ stands for the divergence operator, and will always be applied to vector fields or matrices. It is not restrictive to require W to be symmetric, $\forall z \in \mathbb{R}^d$, $W(-z) = W(z)$.

Here, the velocity field of the equation is nonlinearly related to the probability density itself and given by $u = -\nabla \frac{\delta \mathcal{F}}{\delta \rho}$ with \mathcal{F} being the free-energy or entropy functional:

$$\mathcal{F}(\rho) = \int_{\mathbb{R}^d} U(\rho) dx + \int_{\mathbb{R}^d} V(x) \rho(x) dx + \frac{1}{2} \int_{\mathbb{R}^d \times \mathbb{R}^d} W(x-y) \rho(x) \rho(y) dx dy. \quad (1.2)$$

Actually, this free-energy functional is dissipated along the trajectories of equation (1.1) following the law:

$$\frac{d}{dt} \mathcal{F}(\rho)(t) = -D(\rho) \equiv - \int_{\mathbb{R}^d} |u(t, x)|^2 \rho(t, x) dx, \quad (1.3)$$

where D is called the *entropy dissipation functional*.

Without interaction potential $W = 0$, this general family of equations contain well-known models in mathematical physics such as the heat equation, $U(s) = s \log s$ and $V = 0$, the porous-medium and fast-diffusion equations [56], $U(s) = s^m / (m - 1)$, $m > 0$ and $V = 0$ and their Fokker-Planck counterparts, $U(s) = s \log s$ and $V =$

*ICREA - Departament de Matemàtiques, Universitat Autònoma de Barcelona, 08193 Bellaterra, Spain.

†Departament de Tecnologia, Universitat Pompeu Fabra, Passeig Circumval·lació 8, 08003 Barcelona, Spain.

$|x|^2/2$, and $U(s) = s^m/(m-1)$ and $V = |x|^2/2$ respectively, see [28, 29, 50, 25] for instance.

Models with interaction potential are ubiquitous in many fields ranging from applications in Physics to Mathematical Biology. The equation with $W = |x|^3/3$ and $U = V = 0$ was introduced in [10] as a simplified model of thermalization of inelastic particle systems. Variations of this model with stochastic heating [11], $W = |x|^3/3$, $U = s \log s$, and $V = 0$, and more general interaction potentials [55, 42], $W = |x|^{2+\gamma}/(2+\gamma)$, $\gamma > -1$, have also been considered in this particular application.

Another source of models with interaction potential appears in mathematical biology. Cell movement by chemotaxis has been modeled by systems of equations [51, 40]. Usually, one has an evolution of the density of cells $\rho(t, x)$ coupled to a reaction diffusion equation for the chemical substance $k(t, x)$ that these cells react to:

$$\begin{cases} \frac{\partial \rho}{\partial t}(x, t) = \Delta \rho(x, t) - \chi \nabla \cdot (\rho(x, t) \nabla k(x, t)) & x \in \mathbb{R}^2, t > 0, \\ \frac{\partial k}{\partial t}(x, t) - \Delta k(x, t) = \rho(x, t) - \alpha k(x, t) & x \in \mathbb{R}^2, t > 0. \end{cases}$$

However, it is assumed that the relaxation of chemical concentration happens faster than for the cell density, and then, the time derivative of the concentration is neglected. Assuming that $\alpha = 0$ and expressing the solution of the equation $-\Delta k = \rho$ in terms of convolution with the Newtonian potential in \mathbb{R}^2 , we obtain the well-known Patlak-Keller-Segel (PKS) system, see [31, 17, 24, 15, 16] for more information. Thus, the PKS system corresponds to (1.1) with $U = s \log s$, $V = 0$, and $W = \frac{\chi}{2\pi} \log |x|$ in two dimensions.

Mathematical modeling of swarms, flocks and collective motion of individuals have also been treated by continuum models stemming from particle discrete models [18, 53, 47, 54, 22, 48]. They lead to equations with $W = -e^{-|x|}$, $V = 0$ with or without linear or nonlinear diffusion, $U(s) = s \log s$ or $U(s) = s^m/(m-1)$ with $m > 1$, modeling local repulsive interaction [53, 23]. These continuity equations with nonlocal interaction terms can be deduced from particle systems [34] and they can lead to finite time aggregation of particles [12, 13].

All these continuity equations have a common underlying structure who was first pinpointed in [50] for the porous medium equation. All these equations share the fact that they can be considered as gradient flows with respect to the euclidean Wasserstein distance of the free-energy functional $\mathcal{F}(\rho)$, see [26, 59, 3, 27]. Actually, this structure shows that solutions can be constructed by the variational schemes introduced in [39]. As a consequence, it seems natural to try to solve these variational schemes numerically since they have a built-in positivity and free-energy decreasing property.

These numerical semidiscrete scheme involves in principle the numerical solution of a quite challenging numerical problem, i.e., the Monge-Kantorovich optimal transport map between measures. The numerical solution to this problem is quite costly [9], although there are some recent developments in the field with applications to image processing [7, 8, 38].

This variational scheme has already been used in the one-dimensional case by the numerical community. Here, the reduction to one-dimension is essential since the Wasserstein distance in this case reduces to an L^2 distance of inverses of distribution functions [59, 30]. Moreover, the variational scheme is nothing else than an implicit Euler scheme for the PDE satisfied by the inverse of the distribution function associated to the unknown density, [41] and see [15] for an application of this scheme to

the PKS system. Related schemes have been proposed for the interaction potential equation and nonlinear diffusion keeping some contraction properties [35, 36].

In this work, we propose to solve numerically the system of PDEs satisfied by the diffeomorphism representing the unknown density from constant distribution of mass over the domain. This equation appeared in the study of weak solutions for a very particular class of classical L^2 -gradient flows of functionals on diffeomorphisms in [32] and then further analyzed in [4]. This system of PDEs to compute the evolving diffeomorphism is the equivalent in higher dimensions to the equation satisfied by the inverse distribution function of a density.

This representation has lots of numerical advantages. Since the transport map from constant density sends more points to the places of larger mass concentration, the uniform mesh adapts itself in a natural way to the shape of the mass distribution. On the other hand, aggregation phenomena lead usually to the convergence towards delta-Dirac distributions located at certain points, see the PKS system [57, 58, 16] for instance or [12]. Therefore, this approach allows the tracking of the formation of these singularities and their profile in a smooth natural mesh-adaptive manner. Moreover, the formation of Delta-Diracs appear as a degeneration of the transport maps to be diffeomorphisms which is numerically more tractable than the blow-up of the density in original variables. Also, this method demonstrates good features for the diffusive cases, since it allows the tracking of free boundaries and merging of different mass patches in a natural way. These evolving diffeomorphisms can also be thought as solving equation (1.1) in Lagrangian coordinates by particle methods since the equation solved for the diffeomorphisms can be thought as finding the flow map associated to the velocity field u .

Finally, let us mention that this approach can be recast in a more general setting including equations deriving from free-energy minimization on variational schemes involving optimal transport costs different from the euclidean. In fact, we can also solve in this way, equations of the form:

$$\frac{\partial \rho}{\partial t} = -\nabla \cdot (\rho u_c) := \nabla \cdot \{ \rho \nabla c^* [\nabla (U'(\rho) + V + W * \rho)] \}, \quad (1.4)$$

where c is the cost function in the variational scheme and c^* its Legendre transform. These equations lead to p -Laplacian equations or doubly nonlinear equations with the choice $V = W = 0$, $U(s) = s \log s$ or $U(s) = s^m / (m - 1)$, and $c(x) = |x|^q / q$ with q the conjugate exponent of p , see [49, 1, 2]. Even some flux-limited equations appearing in relativistic flows can be numerically solved with this approach, see [5, 6, 46], in which we want to solve

$$\frac{\partial \rho}{\partial t} = \nabla \cdot \left(\rho \frac{\nabla \rho}{\sqrt{\rho^2 + |\nabla \rho|^2}} \right) = \nabla \cdot \left(\rho \frac{\nabla \log \rho}{\sqrt{1 + |\nabla \log \rho|^2}} \right). \quad (1.5)$$

Here, the cost function is given by

$$c(x) = \begin{cases} 1 - \sqrt{1 - |x|^2} & \text{if } |x| \leq 1 \\ +\infty & \text{if } |x| > 1. \end{cases},$$

for which $c^*(x) = \sqrt{1 + |x|^2} - 1$.

The plan of this paper is the following: in the next section, we will review the main ideas from [32, 4] related to the variational schemes in [39] we need in this work. Section 3 will be devoted to explain the numerical algorithm and the initialization of it. Finally, section 4 will show the numerical experiments in the different situations of aggregation and diffusion discussed in the introduction.

2. Variational Approximations & Evolving Diffeomorphisms. Let $\mu, \nu \in \mathcal{P}(\mathbb{R}^d)$ the space of probability measures in \mathbb{R}^d , $\mathcal{P}_2(\mathbb{R}^d)$ the subset of probability measures with finite second moment, $\mathcal{P}_2^{\text{ac}}(\mathbb{R}^d)$ its subset formed by the absolutely continuous measures with respect to Lebesgue and T be a measurable map $T: \mathbb{R}^d \rightarrow \mathbb{R}^d$. We say that T *transports* μ onto ν and we note $\nu = T\#\mu$ if for any measurable set $B \subset \mathbb{R}^d$, $\nu(B) = \mu \circ T^{-1}(B)$, or equivalently

$$\int_{\mathbb{R}^d} \zeta \circ T(x) \, d\mu(x) = \int_{\mathbb{R}^d} \zeta(y) \, d\nu(y) \quad \forall \zeta \in \mathcal{C}_b^0(\mathbb{R}^d). \quad (2.1)$$

The euclidean Wasserstein distance d_W between μ and ν , d_W can be defined by

$$d_W^2(\mu, \nu) := \inf_{T: \nu=T\#\mu} \int_{\mathbb{R}^d} |x - T(x)|^2 \, d\mu(x).$$

By Brenier's theorem [19, 44, 45], see [59, Theorem 2.32, p.85] for a review, if μ is absolutely continuous with respect to Lebesgue measure, then there is one measurable map T such that $\nu = T\#\mu$ and $T = \nabla\varphi$ for some convex function φ . As a consequence,

$$d_W^2(\mu, \nu) = \int_{\mathbb{R}^d} |x - \nabla\varphi(x)|^2 \, d\mu(x). \quad (2.2)$$

The variational problem leading to the definition of the Wasserstein distance can be relaxed to the linear programming problem:

$$d_W^2(\mu, \nu) = \inf_{\Pi \in \Gamma} \left\{ \int_{\mathbb{R}^d \times \mathbb{R}^d} |x - y|^2 \, d\Pi(x, y) \right\},$$

where Π runs over the set of transference plans Γ , that is, the set of joint probability measures on $\mathbb{R}^d \times \mathbb{R}^d$ with marginals μ and ν . In fact, the infimum above is a minimum by Kantorovich duality theorems [59, Chapter 1]. The optimal transference plan, in case Brenier's theorem applies, is given by $\Pi_o = (id_{\mathbb{R}^d} \otimes \nabla\varphi)\#\mu$.

Associated to this euclidean distance, a variational scheme for the doubly non-linear equation and the heat equation was introduced in [49, 39], and consequently generalized to all the equations of the form (1.1) in [1, 3]. This variational scheme reads as:

$$\rho_{\Delta t}^{n+1} \in \arg \inf_{\rho \in \mathcal{K}} \left\{ \frac{1}{2\Delta t} d_W^2(\rho_{\Delta t}^n, \rho) + \mathcal{F}(\rho) \right\}, \quad (2.3)$$

for a fixed time step $\Delta t > 0$, an initial datum $\rho^0 \in \mathcal{P}_2^{\text{ac}}(\mathbb{R}^d)$ with

$$\mathcal{K} := \left\{ \rho \in L_+^1(\mathbb{R}^d) : \int_{\mathbb{R}^d} \rho(x) \, dx = M, |x|^2 \rho \in L^1(\mathbb{R}^d) \right\}.$$

Here, M is the total mass of the initial data. Let us point out that the normalization of unit total mass is not necessary at all since the total mass is preserved by the continuity equations treated. For simplicity, our densities will be normalized to have total mass M and the transport distance d_W is defined analogously for these positive measures with total mass M .

This steepest descent scheme can be understood [3] as a time discretisation of an abstract gradient flow equation in the space of probability measures. We refer to [50, 59, 3, 27] for a deeper discussion, the heuristics and the rigorous sense of the

gradient flow structure. In [3], it is proved that suitably time interpolation of the solutions of this variational scheme approach the solution of the limiting equations (1.1) at first order in time in the Wasserstein sense.

More general equations (1.4) can be treated by allowing more general distances induced by different cost functionals for the transport of mass from location x to location y . Let us denote by $c(x, y) : \mathbb{R}^d \times \mathbb{R}^d \rightarrow \mathbb{R}^+$ this cost function. Let us assume that c is radially symmetric in the sense of $c(x, y) = c(x - y) = c(|x - y|)$, then the associated variational scheme to equation (1.4) is:

$$\rho_{\Delta t}^{n+1} \in \arg \inf_{\rho \in \mathcal{K}_c} \left\{ \Delta t \inf_{\Pi \in \Gamma(\rho_{\Delta t}^n, \rho)} \left\{ \int_{\mathbb{R}^d \times \mathbb{R}^d} c \left(\frac{x - y}{\Delta t} \right) d\Pi(x, y) \right\} + \mathcal{F}(\rho) \right\}, \quad (2.4)$$

where $\Gamma(\rho_{\Delta t}^n, \rho)$ is the set of measures in the product space $\mathbb{R}^d \times \mathbb{R}^d$ with marginals $\rho_{\Delta t}^n$ and ρ respectively. This variational scheme was proven to be convergent in a very general setting [1, 3, 46] including the p -laplacian equations, the doubly-nonlinear equations and the relativistic heat equation.

Let us finally remark that the whole theory can be recast in a bounded domain and the Cauchy problems obtained have to be complemented with no-flux boundary conditions to keep the total mass constant. We will elaborate further below.

Recently, a connection between the theory of variational steepest descent schemes with respect to the euclidean transport distance and the L^2 -gradient flows of polyconvex functionals on diffeomorphisms was obtained in [32]. Let Ω be a smooth, open, bounded and connected subset of \mathbb{R}^N and let $\tilde{\Omega}$ be an open subset of \mathbb{R}^N . Let us consider the functionals of the form

$$\mathcal{I}(\Phi) = \int_{\Omega} \Psi(\det D\Phi) dx$$

where $\Phi \in \mathcal{D}$, the set of diffeomorphisms from $\bar{\Omega}$ onto $\bar{\tilde{\Omega}}$ which maps $\partial\Omega$ onto $\partial\tilde{\Omega}$. They showed that the classical L^2 -gradient flow:

$$\Phi_{\Delta t}^{n+1} \in \arg \inf_{\Phi \in \mathcal{D}} \left\{ \frac{1}{2\Delta t} \|\Phi_{\Delta t}^n - \Phi\|_{L^2(\Omega)}^2 + \mathcal{I}(\Phi) \right\}, \quad (2.5)$$

is well defined and it converges to a solution of the system of PDEs:

$$\frac{\partial \Phi}{\partial t} = \nabla \cdot [\Psi'(\det D\Phi)(\text{cof } D\Phi)^T], \quad (2.6)$$

where $D\Phi = \left(\frac{\partial \Phi_i}{\partial x_j} \right)$ is the Jacobian matrix of Φ , $\text{cof } A$ is the cofactor matrix and T is the transpose of a matrix, with vectors considered as columns. This result was proved in these particular set of polyconvex functionals since they are related to the variational scheme (2.3). Actually, taking an arbitrary diffeomorphism $\Phi \in \mathcal{D}$ is equivalent to give $\rho \in \mathcal{K}$ by setting $\rho = \Phi \# \mathcal{L}^N \llcorner_{\Omega}$. In fact, due to smoothness, $\rho = \Phi \# \mathcal{L}^N \llcorner_{\Omega}$ is equivalent to

$$\rho(\Phi(x)) \det(D\Phi) = 1 \quad \text{on } \Omega, \quad (2.7)$$

or equivalently $\rho = \det[(D\Phi)^{-1}] \circ \Phi^{-1}$. Using this change of variables on the definition of the functional $\mathcal{F}(\rho)$ with $V = W = 0$, one recovers

$$\mathcal{F}(\rho) = \int_{\tilde{\Omega}} U(\rho) dx = \int_{\Omega} U(\rho(\Phi(x))) \det(D\Phi) dx = \int_{\Omega} \Psi(\det(D\Phi)) dx$$

with $\Psi(s) = sU(1/s)$ for all $s > 0$. Also, if one performs this change of variables on the definition of the transport distance, then

$$\begin{aligned} d_W^2(\rho_{\Delta t}^n, \rho) &:= \inf_{T: \rho = T\#\rho_{\Delta t}^n} \int_{\tilde{\Omega}} |x - T(x)|^2 \rho_{\Delta t}^n(x) \, dx \\ &= \inf_{T: \rho = T\#\rho_{\Delta t}^n} \int_{\Omega} |\Phi_{\Delta t}^n(x) - T(\Phi_{\Delta t}^n(x))|^2 \, dx \\ &= \inf_{\Phi: \rho = \Phi\#\chi_{\Omega}} \int_{\Omega} |\Phi_{\Delta t}^n(x) - \Phi(x)|^2 \, dx \end{aligned}$$

where $\rho_{\Delta t}^n = \Phi_{\Delta t}^n\#\mathcal{L}^N\llcorner_{\Omega}$. These remarks suggest that both schemes are equivalent modulo this change of variables, and this is what is shown in [32] and generalized and improved in [4]. In fact, one can also directly perform the change of variables (2.7) on the nonlinear diffusion equation

$$\frac{\partial \rho}{\partial t} = \nabla \cdot [\rho \nabla U'(\rho)]$$

to conclude (2.6).

Let us generalize this idea. Applying the change of variables (2.7) to (1.1), it is easy to check that one obtains the following system for the evolving diffeomorphisms representing the solution $\rho(t) = \Phi(t)\#\mathcal{L}^N\llcorner_{\Omega}$ at each time $t > 0$:

$$\frac{\partial \Phi}{\partial t} = \nabla \cdot [\Psi'(\det D\Phi)(\text{cof } D\Phi)^T] - \nabla V \circ \Phi - \int_{\Omega} \nabla W(\Phi(x) - \Phi(y)) \, dy := u(t) \star \Phi, \quad (2.8)$$

with a corresponding initial data Φ_o representing $\rho_o = \Phi_o\#\mathcal{L}^N\llcorner_{\Omega}$. In fact, equation (2.8) is the Lagrangian coordinates representation of the original Eulerian formulation (1.1).

This change of variables (2.7) can again be applied to the variational scheme (2.3) to obtain the corresponding variational scheme for the diffeomorphisms of the form (2.5) where

$$\mathcal{I}(\Phi) = \int_{\Omega} \Psi(\det D\Phi) \, dx + \int_{\Omega} V(\Phi(x)) \, dx + \frac{1}{2} \int_{\Omega} \int_{\Omega} W(\Phi(x) - \Phi(y)) \, dx \, dy. \quad (2.9)$$

This idea can be further generalized to variational schemes (2.4) and equations of the form (1.4), giving

$$\nabla c \left(\frac{\partial \Phi}{\partial t} \right) = \nabla \cdot [\Psi'(\det D\Phi)(\text{cof } D\Phi)^T] - \nabla V \circ \Phi - \int_{\Omega} \nabla W(\Phi(x) - \Phi(y)) \, dy. \quad (2.10)$$

or in synthetic manner

$$\frac{\partial \Phi}{\partial t} = \nabla c^*(u(t) \star \Phi),$$

with the associated free energy/entropy functional given by (2.9).

The equations of the form (1.1) and (1.4) when solved in a bounded domain have to be complemented with no-flux boundary conditions:

$$u \cdot \eta = 0 \quad (u_c \cdot \eta = 0) \quad \text{on } \partial\tilde{\Omega} \quad (2.11)$$

with η the outwards unit normal at the boundary of $\tilde{\Omega}$, remember with our notation $u \cdot \eta = u^T \eta$. This allows for the conservation of mass and the decay of the free-energy/entropy for equations (1.1) and (1.4). It is easy to check that formally smooth solutions of (1.1) should satisfy:

$$\frac{d}{dt} \mathcal{F}(\rho(t)) = - \int_{\tilde{\Omega}} \rho(x, t) |u(t, x)|^2 dx.$$

This decreasing property of the free energy functional is trivially preserved in the variational scheme (2.3), since by construction $\mathcal{F}(\rho_{\Delta t}^{n+1}) \leq \mathcal{F}(\rho_{\Delta t}^n)$, for all $n \in \mathbb{N}$. Thus, this property is preserved for the variational scheme of the evolving diffeomorphisms (2.5), giving $\mathcal{I}(\Phi_{\Delta t}^{n+1}) \leq \mathcal{I}(\Phi_{\Delta t}^n)$, for all $n \in \mathbb{N}$. This entropy decreasing property of the variational scheme for (2.8) determines the boundary conditions naturally associated to the system. The boundary condition has to be such that the entropy $\mathcal{I}(\Phi)$ is decreasing along its evolution, and thus, by computing the time-derivative, we get

$$\frac{d}{dt} \mathcal{I}(\Phi(t)) = - \int_{\tilde{\Omega}} |u(t) \star \Phi|^2 dx - \int_{\partial \tilde{\Omega}} \Psi'(\det D\Phi) \eta^T (\text{cof } D\Phi)^T \frac{\partial \Phi}{\partial t} dx$$

from which, we conclude that the natural boundary condition for the system (2.8) associated to the variational scheme (2.5) is:

$$\eta^T (\text{cof } D\Phi)^T \frac{\partial \Phi}{\partial t} = (\text{cof } D\Phi) \eta \cdot \frac{\partial \Phi}{\partial t} = 0 \quad \text{on } \partial \tilde{\Omega}. \quad (2.12)$$

Analogously, the free-energy/entropy dissipation associated to equation (1.4) is:

$$\frac{d}{dt} \mathcal{F}(\rho(t)) = - \int_{\tilde{\Omega}} \rho(x, t) u(t) \cdot u_c(t) dx$$

where $u(t) \cdot u_c(t) = u(t) \cdot \nabla c^*[u(t)] \geq c^*[u(t)] \geq 0$ by convexity of c^* . Therefore, one finds that the boundary condition associated to the generalized diffeomorphisms equation (2.10) is given again by (2.12).

Finally, let us point out that this change of variables (2.7) can be applied to any equation in divergence form, i.e.

$$\frac{\partial \rho}{\partial t} = \nabla \cdot [a(x, \rho, \nabla \rho)], \quad (2.13)$$

giving the following evolution system for the diffeomorphisms

$$\frac{\partial \Phi}{\partial t} = -a \{ \Phi, \det[(D\Phi)^{-1}], (\nabla \det[(D\Phi)^{-1}]) (D\Phi)^{-1} \} \det(D\Phi). \quad (2.14)$$

The main issue here is that there is no variational scheme behind this general kind of equations and therefore, it is not clear what are the right boundary conditions to impose.

3. Numerical methods. In this work, we will deal with the numerical solutions of equations (1.1) and (1.4) in two dimensions. Our numerical method is based on representing solutions in a squared geometry by the evolving diffeomorphisms or Lagrangian coordinates $\Phi(t)$, and thus, we will fix in the sequel $\tilde{\Omega} = [c, d]^2$ as the physical domain and $\Omega = [a, b]^2$ as computational domain, which is not restrictive in many practical applications.

There have been many works in the literature devoted to the analysis of blow-up of solutions for the Schrödinger equation [52], for formation of concentrated regions in compressible flows by adaptive meshes [43], for the concentration problem in chemotactic collapse [20] and for the blow-up problem in semilinear heat equations [21]. The common goal of these works is to obtain a new mesh better adapted to the solution's profile by minimizing certain ad-hoc functional and solving the equations in these new meshes. Let us point out that the closest literature to our present work has been recently proposed in [21]. They suggest to construct moving meshes for blow-up problems in semilinear heat equations by solving a Monge-Ampère equation for finding the meshes. These new meshes fit better the mass distribution of the function to be numerically obtained. In Figure 3.1, one can see the initial data of some tests, a gaussian centered on the square domain $[0, 1]^2$ and a cut parabola and their meshes, the representing diffeomorphisms Φ_0 of these initial data.

Our proposed algorithm also adapts itself in an automatic manner since we solve for the diffeomorphism representing the solutions from constant distribution of mass. However, we avoid finding a solution of the corresponding Monge-Ampère equation as in [21] by solving directly the evolution of these diffeomorphisms. Therefore, the solution of the diffeomorphism equations (2.10) and (2.14) adapt naturally to the concentration or diffusion of mass. This is one of the great numerical advantages of this method. As a drawback, we increase the computational cost of solving numerically a single nonlinear PDE by solving an intricate system of evolutionary nonlinear PDEs. Nevertheless, we can continue solving in the original fixed cartesian mesh the diffeomorphisms equation which is of great computational advantage.

Concerning the boundary conditions (2.12) in a squared geometry they translate to:

$$\frac{\partial \Phi_1}{\partial t} \frac{\partial \Phi_2}{\partial x_2} - \frac{\partial \Phi_2}{\partial t} \frac{\partial \Phi_1}{\partial x_1} = 0 \quad \text{for } x_1 = a, x_1 = b$$

and

$$-\frac{\partial \Phi_1}{\partial t} \frac{\partial \Phi_1}{\partial x_2} + \frac{\partial \Phi_2}{\partial t} \frac{\partial \Phi_1}{\partial x_1} = 0 \quad \text{for } x_2 = a, x_2 = b.$$

Since our diffeomorphism Φ will be mapping $\partial\Omega$ onto $\partial\tilde{\Omega}$, we will restrict to the particular case in which the diffeomorphism maps each edge of $\partial\Omega$ onto the corresponding one of $\partial\tilde{\Omega}$ without rotation. As a consequence, we have

$$\Phi_1(t, x) = c, d \quad \text{for } x_1 = a, x_1 = b \quad \text{and} \quad \Phi_2(t, x) = c, d \quad \text{for } x_2 = a, x_2 = b,$$

respectively. Thus, $\frac{\partial \Phi_1}{\partial t} = 0$ on $x_1 = a, x_1 = b$ and $\frac{\partial \Phi_2}{\partial t} = 0$ on $x_2 = a, x_2 = b$, from which the boundary conditions above simplify to

$$\frac{\partial \Phi_2}{\partial x_1} = 0 \quad \text{for } x_1 = a \text{ or } x_1 = b \quad \text{and} \quad \frac{\partial \Phi_1}{\partial x_2} = 0 \quad \text{for } x_2 = a \text{ or } x_2 = b, \quad (3.1)$$

since there are no reasons why the other component should not depend on time to adapt itself to the evolving mass in the boundary. This particular restriction in the boundary mapping has also been used for solving Monge-Ampère equations in [21].

In summary, we will numerically solve the systems (2.8) or (2.10) posed on square domains $\tilde{\Omega} = [a, b]^2$ with the boundary conditions (3.1).

In order to build an initial diffeomorphism Φ_0 corresponding to ρ_0 for the systems (2.8) or (2.10), we first choose $a = 0$ and $b = \sqrt{M}$, where M is the mass of ρ_0 . Then,

we follow the algorithm proposed in [37] which basically consist on finding a solution of a one-dimensional Monge-Kantorovich problem in the x_1 direction followed by the solution of a family of one-dimensional Monge-Kantorovich problems in the x_2 direction. We define a function $\mathbf{a} : [0, \sqrt{M}] \rightarrow [c, d]$ by the equation

$$\int_c^{\mathbf{a}(x_1)} \int_c^d \rho_0(\eta, x_2) dx_2 d\eta = \sqrt{M}x_1. \quad (3.2)$$

Next, we consider $\mathbf{b} : [0, \sqrt{M}]^2 \rightarrow [c, d]^2$ defined by

$$\int_c^{\mathbf{b}(x_1, x_2)} \rho_0(\mathbf{a}(x_1), \eta) d\eta = \frac{x_2}{\sqrt{M}} \int_c^d \rho_0(\mathbf{a}(x_1), \eta) d\eta, \quad (3.3)$$

and set $\Phi_0(x_1, x_2) := (a(x_1), b(x_1, x_2))$. After differentiating (3.2) with respect to x_1 and (3.3) with respect to x_2 , we see that $\Phi_0 \in \mathcal{D}$ and $\rho_0 = \Phi_0 \# \mathcal{L}^N \llcorner \Omega$.

Let us point out that this choice of domains produces a lack of rotational symmetry for radially symmetric functions, as it can be seen in Figure 3.1, since we are working with diffeomorphisms from a square onto a circle. The initialization procedure gives these flat sides in the x_1 -direction due to the order of integration. We warn the reader that this initial lack of symmetry is the origin of the lack of rotational symmetry for some of the solutions below. A possible way to avoid this problem could be to work in polar coordinates with circles as initial domain that we will study elsewhere.

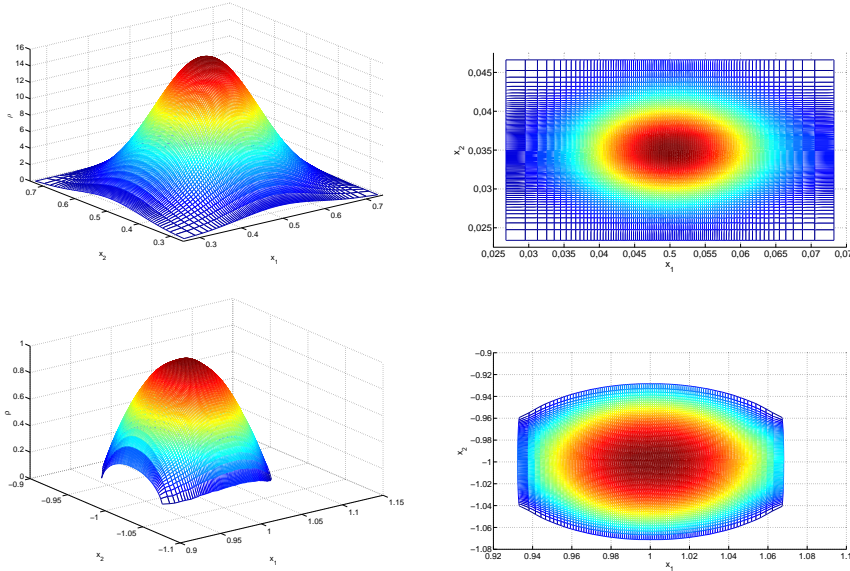


FIG. 3.1. Initial data from two view points where we clearly observe the mesh adaptation. Top: a Gaussian in $[0, 1]^2$; bottom: a cut parabola.

The spatial discretization of this system of PDEs has been treated by simple finite-differences approximations of the derivatives of the unknown Φ involved in the

equation, if the diffusive term appears, together with a numerical composite quadrature formula for the interaction potential integral (Simpson's or trapezoid's rule). Let us precise more our discretization of the diffusive term

$$\nabla \cdot [\Psi'(\det D\Phi)(\text{cof } D\Phi)^T].$$

We first point out that in general $\nabla \cdot [(\text{cof } D\Phi)^T] = 0$, and thus depending on the problem, one can decide to discretize the previous term or the equivalent:

$$(\text{cof } D\Phi)^T \nabla [\Psi'(\det D\Phi)].$$

It is interesting to keep in mind the particular case of linear diffusion for which $\Psi(s) = -\log(s)$, so these terms are

$$-\nabla \cdot [(D\Phi)^{-1}] = -(\text{cof } D\Phi)^T \nabla \left[\frac{1}{\det D\Phi} \right].$$

Let us consider a discretization $\Phi_{i,j}$ on a uniform cartesian grid $\Omega = [a, b]^2$ of Φ with mesh sizes $\Delta x_1 = a/N_1$ and $\Delta x_2 = b/N_2$ respectively. Let us introduce the following notations

$$(D^{\leftarrow}\Phi)_{i,j} = \frac{1}{\Delta x_1}(\Phi_{i,j} - \Phi_{i-1,j}) \quad , \quad (D^{\rightarrow}\Phi)_{i,j} = \frac{1}{\Delta x_1}(\Phi_{i+1,j} - \Phi_{i,j})$$

and

$$(D^{\downarrow}\Phi)_{i,j} = \frac{1}{\Delta x_2}(\Phi_{i,j} - \Phi_{i,j-1}) \quad , \quad (D^{\uparrow}\Phi)_{i,j} = \frac{1}{\Delta x_2}(\Phi_{i,j+1} - \Phi_{i,j}),$$

for all grid points $i = 1, \dots, N_1 - 1, j = 1, \dots, N_2 - 1$.

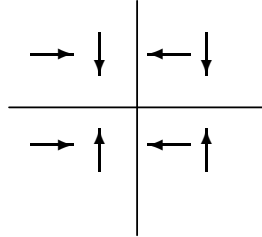


FIG. 3.2. Schematic representation of the order of derivatives approximation with origin at x_c .

Since we are aiming to treat densities ρ which are compactly supported or nearly, then Φ will be a diffeomorphism from Ω onto $\tilde{\Omega}$ but not at the boundary due to the compact support of the target density. Therefore, we have to avoid the use of grid points at the boundaries since $\det D\Phi$ blows up there for compactly supported target densities, see (2.7). This fact also appeared in the one-dimensional schemes developed in [41, 35, 36, 15].

As a consequence, we first decide to choose an even number of discretization points inside the domain, i.e., choose N_1 and N_2 to be odd numbers. We divide the grid into four quadrants with origin at a point x_c to be chosen and take the approximation of the first derivatives appearing in the terms $\Psi'(\det D\Phi)(\text{cof } D\Phi)^T$ dictated by the arrows in each of the four quadrants in Figure 3.2.

To perform the approximation of the divergence operator $\nabla \cdot$, we use the complementary first derivative approximation in each of the quadrants, i.e., if D^\leftarrow was used for the x_1 -derivative approximation, we now use D^\rightarrow and so on. In this way, our approximation gives standard stable centered finite-differences for second derivatives in the same variable. The use of these complementary derivatives needs then some values of the terms in $\Psi'(\det D\Phi)(\text{cof } D\Phi)^T$ at the boundary. Let us discuss just one of the four possibilities of needed values at the boundary, the rest are obtained by symmetries. Let us consider the left two quadrants and the part of boundary $x_1 = a$, then the only derivative involved in $\Psi'(\det D\Phi)(\text{cof } D\Phi)^T$ for which we need a value at the boundary $x_1 = a$ is

$$\Psi'(\det D\Phi) \frac{\partial \Phi_2}{\partial x_2}. \quad (3.4)$$

In principle, we know that $\det D\Phi \rightarrow \infty$ at the boundary and here we will assume that $\Psi'(\infty) = 0$, condition which is satisfied in all the cases mentioned on the introduction and used in this paper. In this way, we assume that $\frac{\partial \Phi_2}{\partial x_2}$ at the boundary $x_1 = a$ is such that $\Psi'(\det D\Phi) \frac{\partial \Phi_2}{\partial x_2}$ at the boundary $x_1 = a$ goes to 0. Under these conditions we then just take zero for the needed values of these terms. Actually, our computation is performed evaluating directly the needed term at the boundary (3.4) with the corresponding approximation of the first derivatives, and thus, we verify numerically that these are really 0 values. In this way, the approximation is coherent too for strictly positive densities. Let us remark that the condition $\Psi'(\infty) = 0$ is equivalent to $f(0+) = 0$ with $f(s) = U(s) - sU'(s)$.

Finally, let us discuss the choice of the point x_c in which the approximation of derivatives reverses the order. We first choose it as the center of one of the mesh rectangles. In principle, we know that at this point there might be a larger discrepancy between the values of the first derivatives approximations to either side of the point, therefore we just choose it in such a way that this discrepancy is the smallest. The global maximum is the natural candidate since there the first derivatives are zero and their derivatives in any or axial directions will be of the same order. This situation corresponds to an inflection point for the components of Φ in which we expect similar values of the second derivative in the symmetry direction both from the left and right.

We proceed by an explicit time discretization of the problem with the explicit Euler scheme as the default algorithm in case the diffusive term appears in the equation or with high-order explicit Runge-Kutta schemes in case that this diffusive term is not present. This is due to the fact that if $U = 0$, the discretized diffeomorphisms equations can be seen as a set of ODEs, actually a particle method, and thus we want a numerical method with a larger absolute stability region to keep the long-time asymptotics of the system better. Of course, the best would be to use an implicit method but we avoided it in this work to speed up computations.

In case the diffusive term is present, we have a CFL-type condition. In fact, this issue was already studied in the one-dimensional case [35], in which a CFL condition is imposed to keep the diffeomorphism character of the map, an strictly increasing function in their case, along the evolution. In our situation, this can be seen as a standard CFL condition for explicit discretizations of the second-order terms involved in $\nabla \cdot [\Psi'(\det D\Phi)(\text{cof } D\Phi)^T]$. In fact, all the four terms included in the two-dimensional case of $\nabla \cdot [\Psi'(\det D\Phi)(\text{cof } D\Phi)^T]$ are of the form

$$\frac{\partial}{\partial x_k} \left[\Psi'(\det D\Phi) \frac{\partial \Phi_i}{\partial x_j} \right]$$

where $i, j, k = 1, 2$. The reported spatial discretization of these terms leads to a CFL condition of the type

$$\|\Psi'(\det D\Phi)\|_{L^\infty} \frac{\Delta t}{\Delta x^2} \leq \frac{1}{\alpha}$$

with $\alpha \geq 2$ where $\Delta x = \max(\Delta x_1, \Delta x_2)$. This condition reduces to the one in [35, Lemma 3.1] checking it carefully. All the results reported in this work were performed with $\alpha = 8$.

4. Numerical Results. Here, we first start with some test problems for our scheme: the heat equation $U(s) = s \log s$, $V = W = 0$, and the linear Fokker-Planck equation $U(s) = s \log s$, $V = |x|^2/2$ and $W = 0$, posed on square domains with Neumann boundary conditions. Mass is preserved for both equations and their asymptotic tendency is to equilibrate exponentially fast towards equilibrium, a constant density for the heat equation and a gaussian density for the linear Fokker-Planck equation. In Figures 4.1 and 4.2 we have the resulting evolution at different time-steps where we observe the adaptation of the mesh to the mass distribution and the asymptotic equilibration as described above validating the numerical solver for this problem. It is remarkable that the entropy in both cases decays exponentially, up to consistency error in log scale not shown in the figures, although the scheme has not been designed with this purpose.

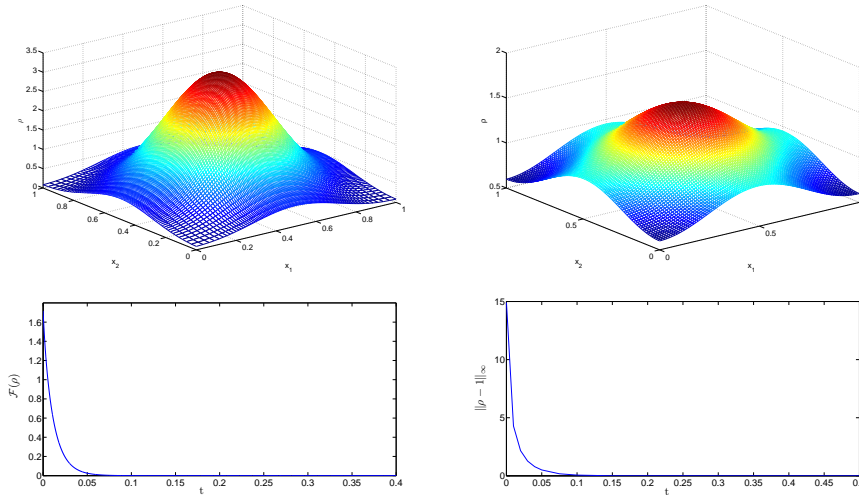


FIG. 4.1. *Evolution of the heat equation with the centered gaussian in $[0, 1]^2$ as initial data: top left at $t = 0.02$, top right at $t = 0.05$, bottom left shows the evolution of entropy $\mathcal{F}(\rho)$, bottom right shows the difference to the constant state in L^∞ norm.*

Another set of test problems are purely aggregation equations with a given confining potential. We choose then $U(s) = 0$, $V = |x|^2/2$ and $W = 0$ in Figure 4.3 and $U(s) = 0$, $V = |x|^3/3$ and $W = 0$ in Figure 4.4. In both cases, the asymptotic behavior is a Dirac delta with the whole mass of the system concentrated at the unique global minimum of the potential, i.e. at the origin. The main difference is that the equilibration velocity depends on the convexity of the potential near the origin as proved in [27]. More precisely, it is proved in [27] that given $V(x) = k_V|x|^{a+2}/(a+2)$ with

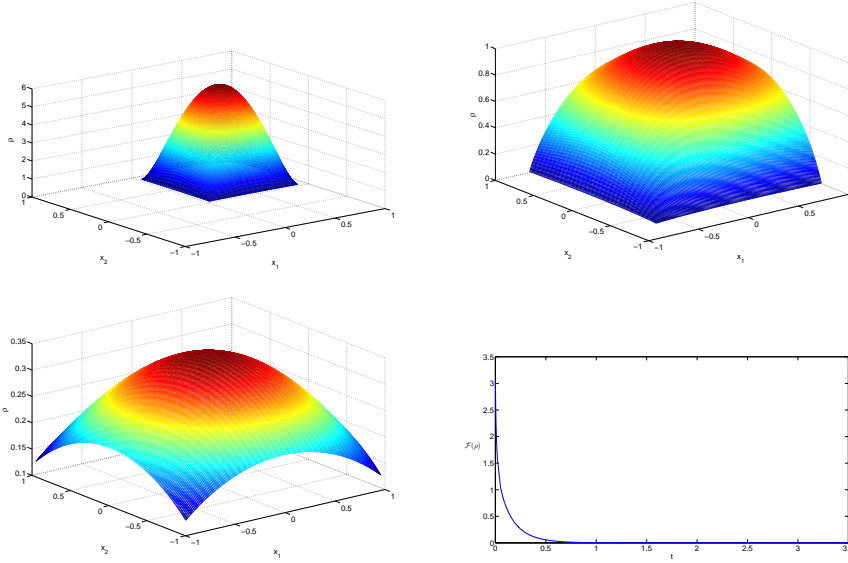


FIG. 4.2. Evolution of the linear Fokker-Planck equation with a cut parabola centered at $(0.5, 0.5)$ in $[-1, 1]^2$ as initial data: top left at $t = 0.01$, top right at $t = 0.5$, bottom left at $t = 3.5$, bottom right shows the evolution of entropy $\mathcal{F}(\rho)$.

$k_V \geq 0$ and $a \geq 0$, the Wasserstein L^2 distance $d_t := d_2(\rho_1(t), \rho_2(t))$ between any two solutions decays like

$$d_t \leq \begin{cases} e^{-k_V t} d_0 & a = 0 \\ d_0(1 + k_V t a (d_0/2)^a)^{-1/a} \sim 2(k_V t a)^{-1/a} & a > 0 \end{cases} \quad (4.1)$$

In both Figures 4.3 and 4.4 we observe the convergence towards the unique stationary point, the Dirac delta at the origin, with the speeds theoretically proven.

Moreover, we discover an interesting feature of the cubic case, it seems that the distribution has an intermediate asymptotic behavior before reaching the total mass concentration. In fact, it seems to concentrate first along an sphere centered at the origin in a self-similar way before final aggregation at the origin. Results of this type are known for nonlinear friction equations with $U = V = 0$ and $W = |x|^3/3$ but it seems unreported for confining potentials. We numerically checked this behavior for centered at the origin initial data. For not centered initial data this concentration on a sphere seems to happen but it seems in a non uniform way, figures not included.

4.1. Numerical Results: Diffusion-type problems. Now, let us concentrate in the family of particular diffusive problems of the form:

$$\begin{cases} \frac{\partial \rho}{\partial t} = \nabla \cdot \left[|\nabla \rho^m|^{p-2} \nabla \rho^m \right], & x \in \Omega \subset \mathbb{R}^d, t > 0 \\ \rho(t=0) = \rho_0, & x \in \Omega \subset \mathbb{R}^d \end{cases} \quad (4.2)$$

with no-flux boundary conditions if posed in a bounded domain and $1 < p < \infty$, $m \geq m_c := \frac{d-p}{d(p-1)}$. This family appears taking $V = W = 0$, the cost given by

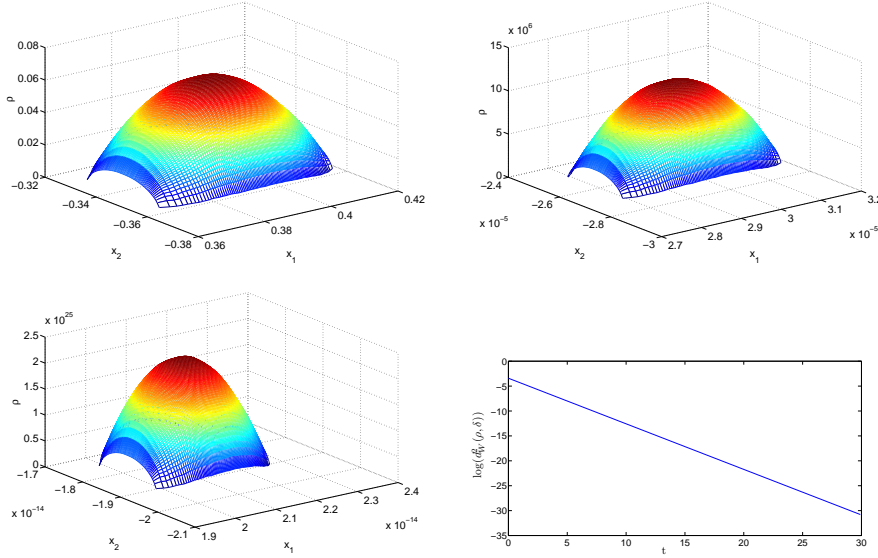


FIG. 4.3. *Evolution of the confining potential case: $U(s) = 0$, $V = |x|^2/2$ and $W = 0$ with a cut parabola centered at $(-1, 1)$ in $[-10, 10]^2$ as initial data: top left at $t = 1$, top right at $t = 10$, bottom left at $t = 30$, bottom right shows the evolution of square of the distance to the stationary Dirac Delta at the origin in log scale.*

$c(x) = |x|^q/q$ with q the conjugate exponent of p and the internal energy given by

$$U(s) = \begin{cases} \frac{1}{p-1} s \ln s & \text{if } m = \frac{1}{p-1} \\ \frac{ms^\gamma}{\gamma(\gamma-1)}, \gamma = m + \frac{p-2}{p-1} & \text{if } m \neq \frac{1}{p-1}. \end{cases}$$

As particular cases, we have the porous medium equation and the p -Laplacian equations. Concerning their asymptotic properties we know that these diffusive equations in bounded domains with Neumann boundary conditions equilibrate to the average of the initial data while in the whole space they evolve towards self-similar states given by Barenblatt-type profiles.

Moreover, the regularity at the boundary of their support/decay properties at the boundary of the domain depend on both m and p and depending whether we are in the finite speed of propagation range $m(p-1) > 1$ or the fast-diffusion range $m(p-1) < 1$. Actually, the Barenblatt self-similar solution is given by

$$\rho_B(t, x) = \frac{1}{t^{d/\delta_p}} u_B\left(\frac{x}{t^{1/\delta_p}}\right), \quad (4.3)$$

where $\delta_p := d(p-1)(m-m_c) > 0$ and

$$u_B(y) = \begin{cases} \frac{1}{\sigma} \exp\left(-\frac{p-1}{q}|y|^q\right) & \text{if } m = \frac{1}{p-1} \\ \left(D_* - \frac{m(p-1)-1}{mp}|y|^q\right)_+^{\frac{p-1}{m(p-1)-1}} & \text{if } m \neq \frac{1}{p-1}, \end{cases} \quad (4.4)$$

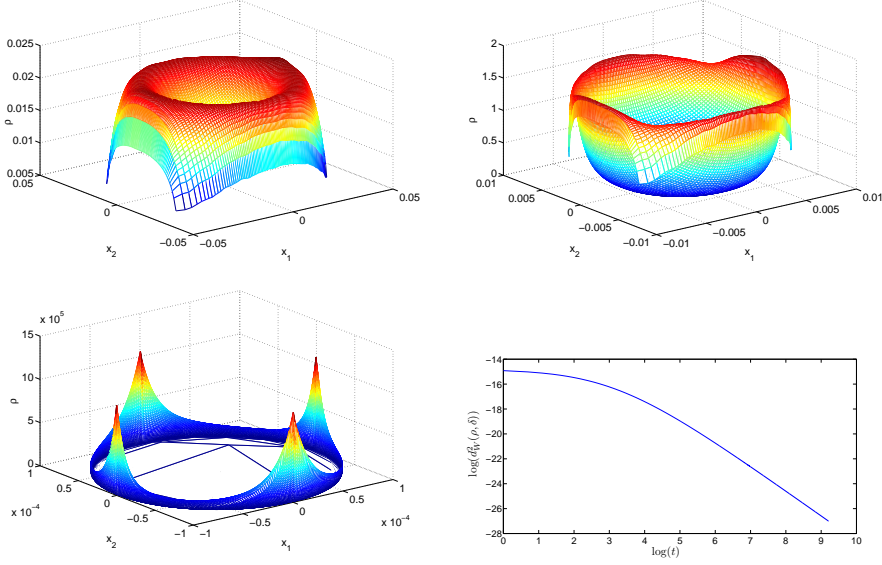


FIG. 4.4. Evolution of the confining potential case: $U(s) = 0$, $V = |x|^3/3$ and $W = 0$ with a cut parabola centered at $(0, 0)$ in $[-10, 10]^2$ as initial data: top left at $t = 10$, top right at $t = 100$, bottom left at $t = 10000$, bottom right shows the log-log plot of the evolution of square of the distance to the stationary Dirac Delta at the origin.

and σ or D_* are uniquely determined by the mass conservation: $\|u_B\|_{L^1(\mathbb{R}^d)} = \|\rho_B(t)\|_{L^1(\mathbb{R}^d)} = \|\rho_0\|_{L^1(\mathbb{R}^d)} = 1$.

In Figure 4.5 we see the evolution starting from a centered gaussian in $[-100, 100]^2$ at different times and values of m and p . In all cases, the equilibration towards constant values and the decay of the energy associated is found numerically in a similar way to the heat equation. We can observe the different shapes of the profiles similar to the ones assumed by the Barenblatt profiles in (4.4) before they are deformed due to the Neumann boundary condition.

We can further check the evolution towards self-similarity in the porous medium case $m = 2$ and $p = 2$ by taking a cut parabola $-|x|^2$ centered at $(-1, 1)$ in a large domain such as $[-10, 10]^2$. Since the solutions remain compactly supported with growing supports in time, the evolution will not be affected by the Neumann boundary conditions for large time intervals to observe the self-similar behavior. Indeed, in Figure 4.6 we observe that evolution and the diameter of the support that increases algebraically as $t^{1/4}$ up to the time, after 10^6 , in which the solution touches the boundary and then is deformed to its average value. Moreover, the decay of the maximum is shown to be as $t^{-1/2}$ as theoretically expected.

We finally check the merging of different mass patches in the porous medium equation with $m = 1.5$ and $p = 2$ by taking three different cut parabolas starting with disjoint supports. The scheme is capable of resolving the evolution and merging of the patches by the following procedure: we evolve each patch independently by its corresponding diffeomorphism to an square domain; giving a "touching" criteria, we perform a merging of the meshes to initialize a new square domain with two joined patches, this algorithm is repeated for each merging event. In this particular example

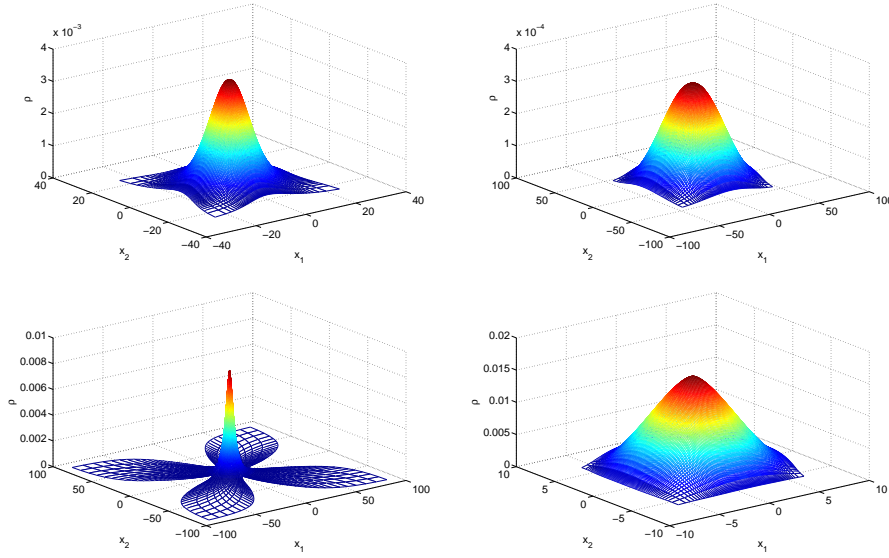


FIG. 4.5. Evolution of the diffusive equation (4.2) with a gaussian centered at $(0,0)$ in $[-100, 100]^2$ as initial data: top left $m = 0.8$ and $p = 2$ at $t = 10$, top right $m = 1.2$ and $p = 2$ at $t = 1000$, bottom left $m = 1$ and $p = 1.5$ at $t = 1$, bottom right $m = 1$ and $p = 3$ at $t = 1000$.

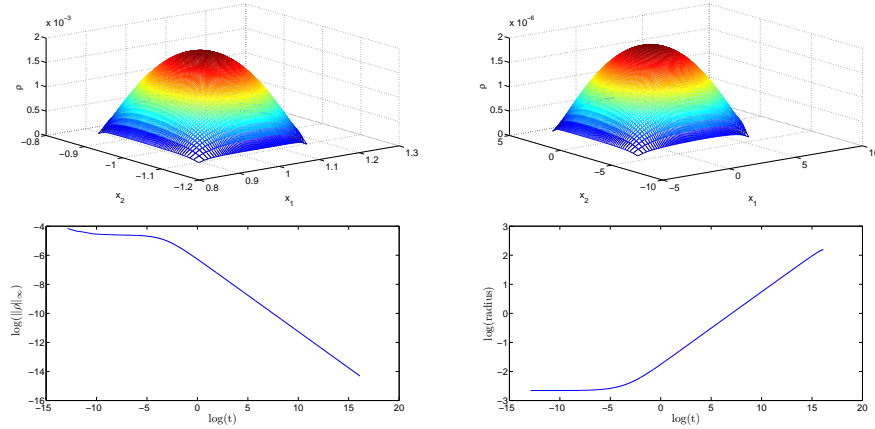


FIG. 4.6. Evolution of the porous medium equation $m = 2$ with a cut parabola centered at $(-1, 1)$ in $[-10, 10]^2$ as initial data: top left at $t = 1$, top right at $t = 10^6$, bottom left log-log-plot of the evolution of $\|\rho\|_\infty$ bottom right the log-log-plot of the evolution of the radius of the solution support.

the dimensions of the meshes of each patch were well prepared to avoid interpolation in the merging step. The "touching" criteria to join patches is as follows: we consider two patches touch when the closest points in their independent evolution are below certain tolerance.

Finally, we have solved numerically with this procedure the relativistic heat equa-

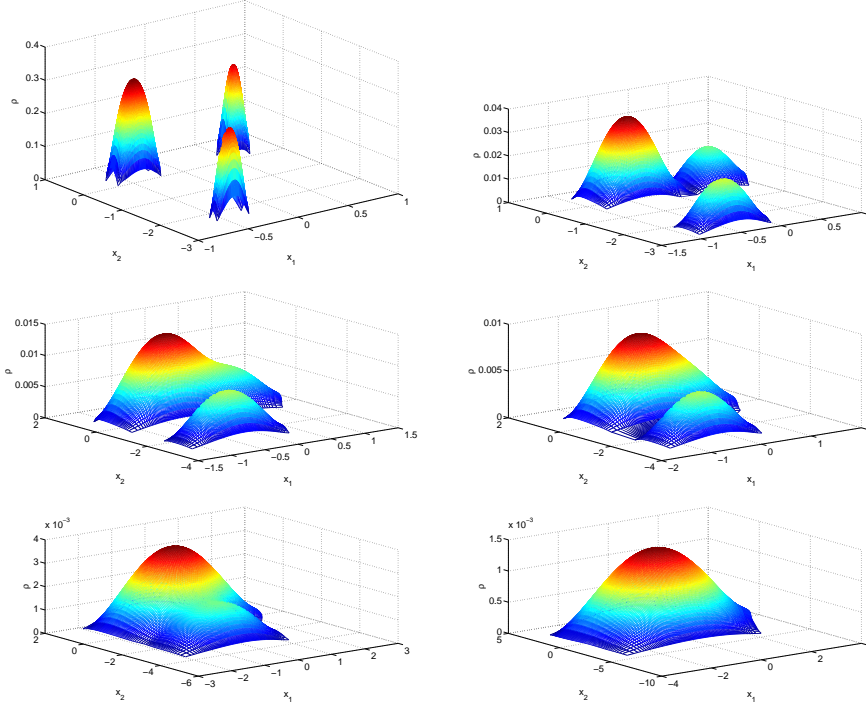


FIG. 4.7. Evolution of three patches for the porous medium equation with $m = 1.5$ in $[-10, 10]^2$: from top left to bottom right at $t = 0.001$, $t = 0.1$, $t = 0.5$, $t = 1.02$, $t = 5$ and $t = 25$ respectively.

tion

$$\frac{\partial \rho}{\partial t} = \nabla \cdot \left(\rho \frac{\nabla \rho}{\sqrt{\rho^2 + |\nabla \rho|^2}} \right) = \nabla \cdot \left(\rho \frac{\nabla \log \rho}{\sqrt{1 + |\nabla \log \rho|^2}} \right).$$

with four picked gaussians as initial data in Figure 4.8. We observe the formation and evolution of sharp profiles and the merging of the different mass packets into one before the eventual relaxation towards constant density. Further properties of these schemes for flux-limited diffusions will be analyzed elsewhere.

4.2. Numerical Results: Aggregation-type problems. In this subsection, we will deal with cases in which the interaction potential plays a leading role. In general, for the problem (1.1) with no diffusion $U = 0$, no confining $V = 0$ and interaction potential of the form $W(x) = k_W |x|^{a+2}/(a+2)$ with $k_W \geq 0$ and $a \geq 0$, the Wasserstein L^2 distance $d_t := d_2(\rho_1(t), \rho_2(t))$ between any two solutions of (1.1) in the whole space decays like

$$d_t \leq \begin{cases} e^{-k_W t} d_0 & a = 0 \\ d_0 (1 + k_W t a (d_0 / \sqrt{2})^a)^{-1/a} \sim \sqrt{2} (k_W t a)^{-1/a} & a > 0, \end{cases}$$

provided the center of masses of the two solutions coincide at each point in time as shown in [27]. Equal center of mass is ensured for example, by assuming reflection symmetry $\Omega = -\Omega$ and $\rho_0(x) = \rho_0(-x)$ initially (and hence for all time).

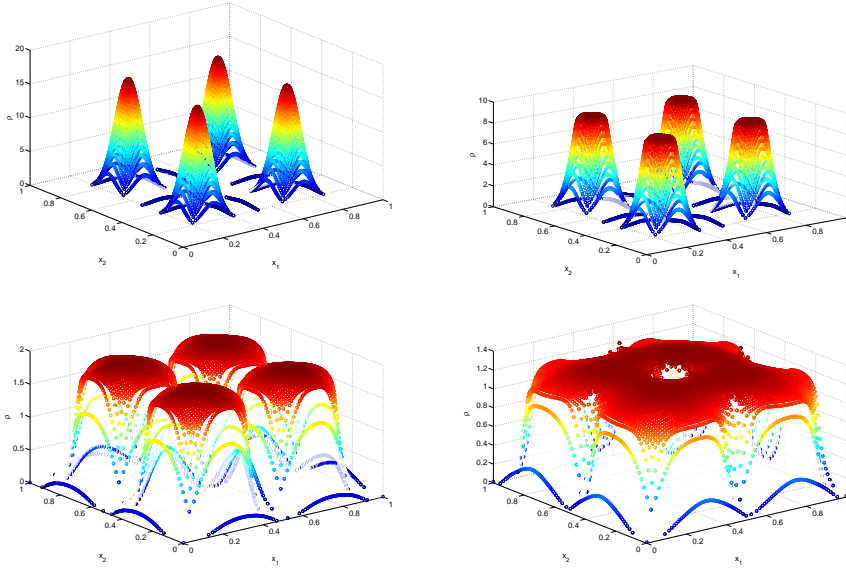


FIG. 4.8. *Evolution of the relativistic heat equation in $[-1, 1]^2$ with four-picked Gaussians as initial data: top left at initial time, top right at $t = 0.5$, bottom left at $t = 0.1$, bottom right at $t = 0.15$.*

This family of equations include the one dimensional model for granular media introduced in [10] in which the external potential is chosen to be cubic, $a = 1$. In this case, it is known that solutions will converge to a delta Dirac in their center of mass with speed given by t^{-1} measured in Wasserstein distance d_2 . Moreover, in one dimension it was shown [10] that the intermediate asymptotics of it is given by two Delta dirac self-similar measure. Some results in higher dimension were obtained by [14] where distributions concentrated in symmetric configurations around the origin were considered as possible intermediate asymptotics of this problem. Actually, in Figure 4.9, we observe this convergence towards a concentrated mass at the origin with the right speed and the tendency of the distribution to concentrate on a self-similar shrinking sphere before achieving the concentration at the origin.

As we discussed in the introduction, several mathematical models of swarms lead to problems of the form (1.1) with $W = -e^{-|x|}$, $V = 0$ with or without linear or nonlinear diffusion, $U(s) = s \log s$ or $U(s) = s^m / (m - 1)$ with $m > 1$, modeling local repulsive interaction [53, 23]. In the absence of diffusive terms, they have been proved to produce finite time aggregation of particles [12, 13].

We conclude from Figure 4.10, that starting from a cut parabola centered at the origin, the solution seems to have a blow-up behavior as a Delta Dirac at the origin with still some mass left outside this Delta evolving smoothly towards the origin. It is quite impressive that the decay of the Wasserstein distance towards the Delta Dirac at the origin is linearly decreasing with unit speed as one should expect from the behavior of the interaction potential $W(x) \simeq |x|$ near the origin implying that particles concentrate with unit speed towards the origin. Similar results for potentials of the form $W(x) = |x|^{\alpha+1}$ with $0 < \alpha < 1$ were reported in [55, 42].

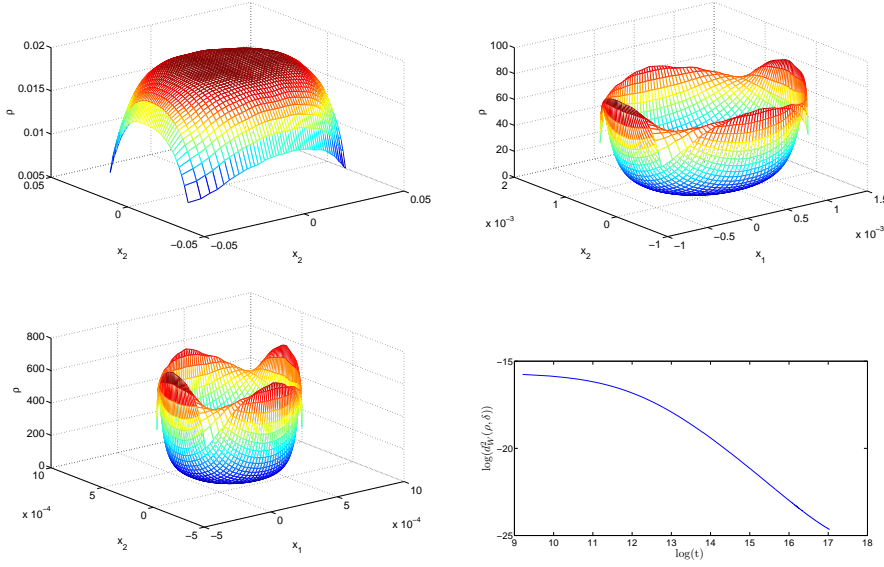


FIG. 4.9. Evolution of the granular media equations with cubic interaction potential in $[-10, 10]^2$ with a centered parabola at the origin as initial data: top left at $t = 10^5$, top right at $t = 10^7$, bottom left at $t = 2.5 \cdot 10^7$, bottom right the log-log plot of the evolution of the d_2 distance towards the Dirac Delta at the origin.

4.3. Numerical Results: Aggregation versus Diffusion problems. Now, we will deal with problems in which there is a struggle between an aggregation and a diffusive mechanism in the problems. For instance, we can start with the granular media model with cubic interaction potential. Introducing a heat bath in the system in the form of an stochastic heating or thermostat between the inelastic interactions, one can produce nontrivial stationary states on the system. This fact was proven in the one-dimensional case in [11] and generalized to any dimension in [26]. More precisely, it was proven that by introducing linear diffusion a non concentrated smooth stationary state is produced and convergence towards it happens exponentially fast [26]. This can be seen in Figure 4.11 where the asymptotic equilibration is demonstrated and the exponential convergence speed is observed.

Concerning the swarming system, we can use our scheme adding linear or nonlinear diffusion to check if its anti-concentration mechanism overcomes that of the aggregation or not. We have simulated the swarming model above with linear diffusion $U(s) = s \log s$ or nonlinear diffusion $U(s) = s^2/2$. The nonlinear diffusion with $m = 2$ is the typical case considered in [53] since it comes from the limiting case of localized repulsion effects. We observe in both cases that the diffusion mechanism wins in the long run, and thus, the density becomes homogenized in the domain converging towards its average value. This is shown in Figure 4.12 with linear diffusion with initial value giving by the concentrated state obtained as the computed density in the final time $t = 26.58174281257$ close to collapse in Figure 4.10.

Finally, let us consider the case of the parabolic-elliptic Patlak-Keller-Segel model in chemotaxis corresponding to (1.1) with $U = s \log s$, $V = 0$, and $W = \frac{\chi}{2\pi} \log |x|$ in two dimensions. In this problem, it is known that the condition $\chi M_c = 8\pi$ gives a

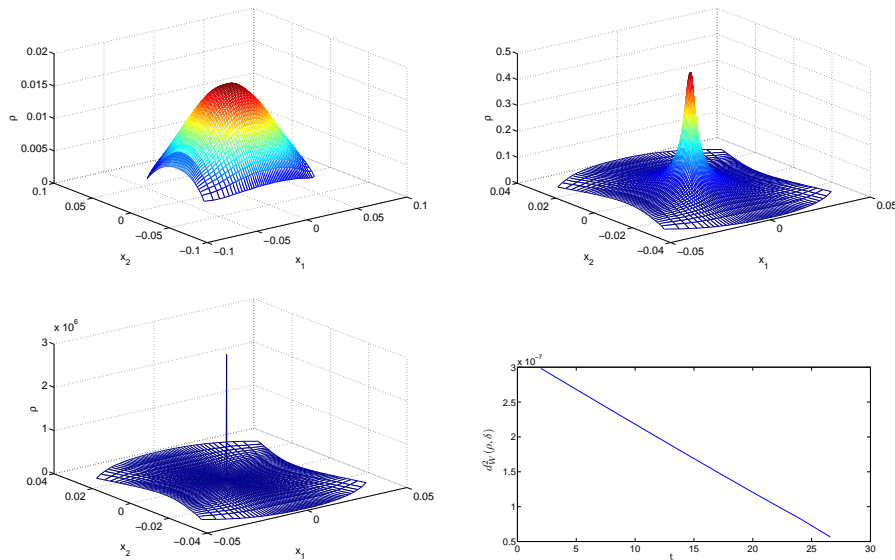


FIG. 4.10. Evolution of the swarming model in $[-10, 10]^2$ with a centered parabola at the origin as initial data: top left at $t = 10$, top right at $t = 26$, bottom left at $t = 26.58174281257$, bottom right the evolution of the d_2 distance towards the Dirac Delta at the origin.

critical mass M_c below which the diffusion wins and above which we have finite time blow-up. We refer to [57, 31, 17, 16] for a deep explanation of this dichotomy result. We show the results for a subcritical case in which $\chi M = 7\pi$ and thus we observe the evolved density at $t = 500$ clearly diffusing in space. We also observe a clear blow-up for a supercritical case in which $\chi M = 9\pi$ in which most of the mass is at center while some mass is left outside. The asymmetry observed in the blow-up profile seems due to the discussion done above in the initialization and the choice of the domain. We will perform a deeper study of the results in the supercritical case elsewhere.

We finally show the results in the case of the chemotaxis problem in two dimensions with nonlinear diffusion in Figure 4.14. In this case, it was proved in [24] that solutions do not blow-up in finite time for any value of the mass if the nonlinear diffusion is of porous-medium type $m > 1$. We observe this fact numerically but furthermore, we observe a convergence towards seemingly stationary compactly supported solutions of the problem. This fact has been thoroughly checked for different mass values and exponents. This asymptotic equilibration to steady distributions has not been yet proven.

Acknowledgements: The authors acknowledge partial support from the projects MTM2008-06349-C03-03, MTM2006-14836 and MTM2008-03176 from DGI-MCI (Spain). We also thank IPAM (UCLA) where part of this work was done and for partial support and Y. Brenier and V. Caselles for useful discussions and encouragements. The authors were also partially supported by ARO grant W911NF-05-1-0112 and ONR grant N000140610059 from A. Bertozzi.

REFERENCES

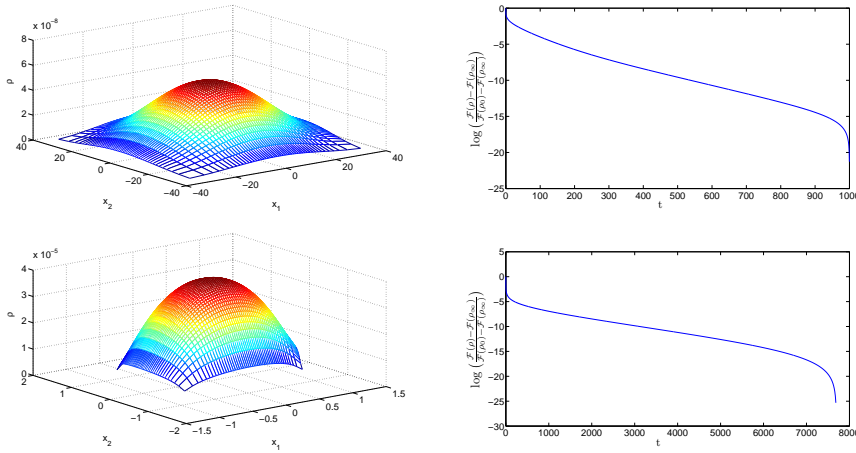


FIG. 4.11. Evolution of the granular media model with cubic interaction potential in $[-100, 100]^2$ with a centered parabola at the origin as initial data: top left asymptotic profile for linear diffusion achieved at $t = 1000$, top right log-plot of the evolution of the relative entropy, bottom left asymptotic profile for nonlinear diffusion ($m=2$) achieved at $t = 8000$, bottom right the log-plot of the evolution of the relative entropy in this case.

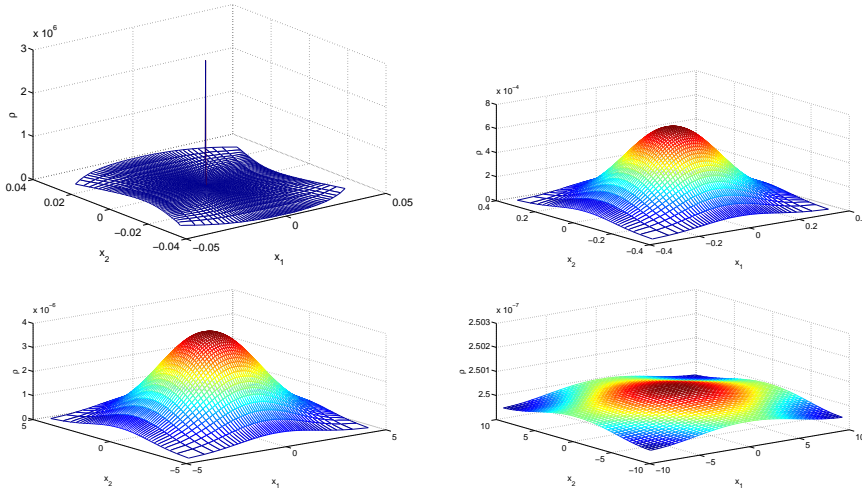


FIG. 4.12. Evolution of the swarming model with linear diffusion in $[-10, 10]^2$ with a centered parabola at the origin as initial data: top left at $t = 0$, top right at $t = 0.0112$, bottom left at $t = 2$, bottom right at $t = 100$.

[1] M. AGUEH, *Existence of solutions to degenerate parabolic equations via the Monge-Kantorovich theory*, Adv. Differential Equations., 10, No 3 (2005), pp. 309-360.
 [2] M. AGUEH, *Rates of decay to equilibria for p -Laplacian type equations*, Nonlinear Anal., 68 (2008), pp. 1909-1927.
 [3] L.A. AMBROSIO, N. GIGLI AND G. SAVARÉ, *Gradient flows in metric spaces and in the space of probability measures*, Lectures in Mathematics, Birkhäuser, 2005.
 [4] L.A. AMBROSIO, S. LISINI AND G. SAVARÉ, *Stability of flows associated to gradient vector fields and convergence of iterated transport maps*, Manuscripta Math, 121 (2006), pp. 1-

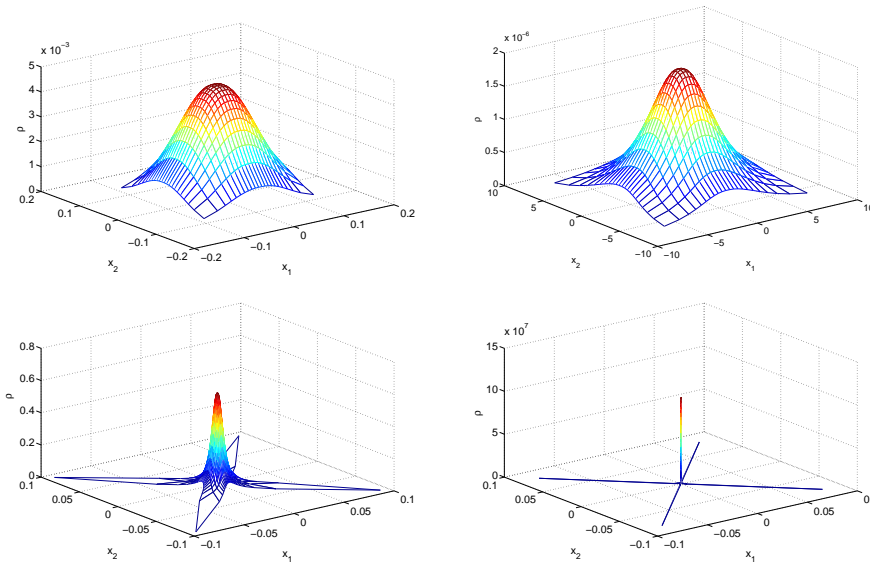


FIG. 4.13. Evolution of the Patlak-Keller-Segel model with linear diffusion in $[-10, 10]^2$ with a centered parabola at the origin as initial data: top left initial data, top right $\chi M = 7\pi$ at $t = 500$, bottom left $\chi M = 9\pi$ at $t = 0.025$, bottom right $\chi M = 9\pi$ at $t = 0.02586440688$.

50.

- [5] F. ANDREU, V. CASELLES, J.M. MAZÓN AND J.S. MOLL, *Finite propagation speed for limited flux diffusion equations*, Arch. Ration. Mech. Anal., 182 (2006), pp. 269–297.
- [6] F. ANDREU, V. CASELLES, J.M. MAZÓN AND J.S. MOLL, *A diffusion equation in transparent media*, J. Evol. Equ., 7 (2007), pp. 113–143.
- [7] S. ANGENENT, S. HAKER AND A. TANNENBAUM, *Minimizing flows for the Monge-Kantorovich problem*, SIAM J. Math. Anal., 35 (2003), 61–97.
- [8] S. ANGENENT, E. PICHON AND A. TANNENBAUM, *Mathematical methods in medical image processing*, Bull. Amer. Math. Soc., 43 (2006), pp. 365–396.
- [9] J.D. BENAMOU, Y. BRENIER, *A computational Fluid Mechanics solution to the Monge-Kantorovich mass transfer problem*, Numer. Math., 84 (2000), pp. 375–393.
- [10] D. BENEDETTO, E. CAGLIOTI, M. PULVIRENTI, *A kinetic equation for granular media*, RAIRO Modél. Math. Anal. Numér., 31, (1997), 615–641.
- [11] D. BENEDETTO, E. CAGLIOTI, J.A. CARRILLO, M. PULVIRENTI, *A non-maxwellian steady distribution for one-dimensional granular media*, J. Stat. Phys., 91, (1998), pp. 979–990.
- [12] A. BERTOZZI AND T. LAURENT, *Finite-time blow-up of solutions of an aggregation equation in \mathbf{R}^n* , Comm. Math. Phys., 274 (2007), pp. 717–735.
- [13] A. BERTOZZI, J.A. CARRILLO AND T. LAURENT, *Blowup in multidimensional aggregation equations with mildly singular interaction kernels*, preprint UAB, (2008).
- [14] M. BISI AND G. TOSCANI, *Self-similar solutions of a nonlinear friction equation in higher dimensions*, Ann. Univ. Ferrara Sez. VII (N.S.), 50 (2004), pp. 91–110.
- [15] A. BLANCHET, V. CALVEZ AND J.A. CARRILLO, *Convergence of the mass-transport steepest descent scheme for the subcritical Patlak-Keller-Segel model*, SIAM J. Numer. Anal., 46 (2008), pp. 691–721.
- [16] A. BLANCHET, J. A. CARRILLO, AND N. MASMOUDI, *Infinite Time Aggregation for the Critical Patlak-Keller-Segel model in \mathbf{R}^2* , Comm. Pure Appl. Math., 61 (2008), pp. 1449–1481.
- [17] A. BLANCHET, J. DOLBEAULT, AND B. PERTHAME, *Two-dimensional Keller-Segel model: optimal critical mass and qualitative properties of the solutions*, Electron. J. Differential Equations, (2006), No. 44, 32 pp. (electronic).
- [18] S. BOI, V. CAPASSO AND D. MORALE, *Modeling the aggregative behavior of ants of the species *Polyergus rufescens**, Spatial heterogeneity in ecological models (Alcalá de Henares, 1998),

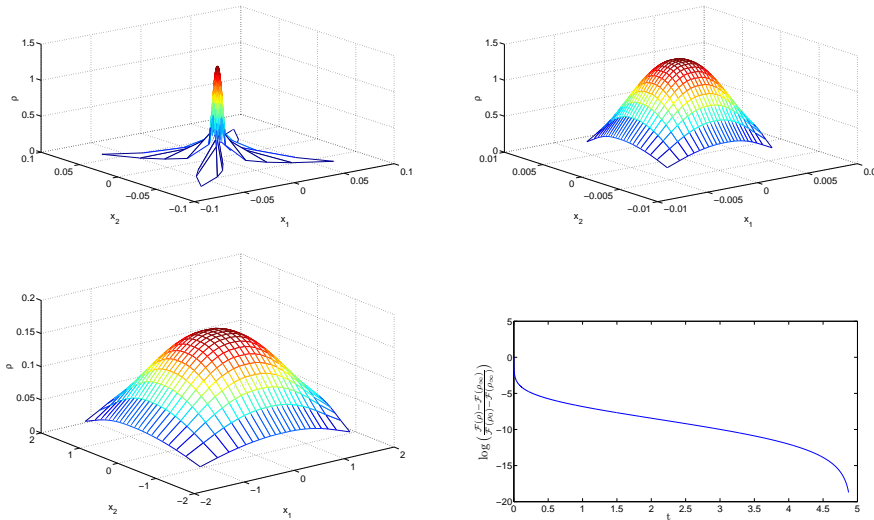


FIG. 4.14. Evolution of the Patlak-Keller-Segel model with nonlinear diffusion ($m = 2$) in $[-10, 10]^2$: top left: evolution of the initial data considered in Figure 4.13 for $\chi M = 10\pi$ at $t = 0.002$, top right: asymptotic profile achieved at $t = 0.0034$, bottom left: asymptotic profile of the evolution of a centered gaussian for $\chi M = \pi$, achieved at $t = 5$, bottom right: log-plot of the evolution of the relative entropy in this latter case.

Nonlinear Anal. Real World Appl., 1 (2000), pp. 163–176.

- [19] Y. BRENIER, *Polar factorization and monotone rearrangement of vector-valued functions*, Comm. Pure Appl. Math. 44, (1991), pp. 375–417.
- [20] C.J. BUDD, R. CARRETERO-GONZÁLEZ AND R.D. RUSSELL, *Precise computations of chemotactic collapse using moving mesh methods*, J. Comput. Phys. 202, (2005), pp. 463–487.
- [21] C.J. BUDD AND J.F. WILLIAMS, *Moving mesh generation using the Parabolic Monge-Ampère equation*, preprint (2008), Internet: <http://people.bath.ac.uk/mascjb/>.
- [22] M. BURGER, V. CAPASSO AND D. MORALE, *On an aggregation model with long and short range interactions*, Nonlinear Analysis. Real World Applications. An International Multidisciplinary Journal, 8 (2007), pp. 939–958.
- [23] M. BURGER AND M. DI FRANCESCO, *Large time behavior of nonlocal aggregation models with nonlinear diffusion*, to appear in Networks and Heterogenous Media.
- [24] V. CALVEZ AND J.A. CARRILLO, *Volume effects in the Keller-Segel model: energy estimates preventing blow-up*, Journal Mathématiques Pures et Appliquées, 86 (2006), pp. 155–175.
- [25] J.A. CARRILLO, A. JÜNGEL, P.A. MARKOWICH, G. TOSCANI AND A. UNTERREITER, *Entropy dissipation methods for degenerate parabolic problems and generalized Sobolev inequalities*, Monatsh. Math., 133 (2001), pp. 1–82.
- [26] J.A. CARRILLO, R.J. MCCANN AND C. VILLANI, *Kinetic equilibration rates for granular media and related equations: entropy dissipation and mass transportation estimates*, Rev. Matemática Iberoamericana, 19 (2003), pp. 1–48.
- [27] J.A. CARRILLO, R.J. MCCANN AND C. VILLANI, *Contractions in the 2-Wasserstein length space and thermalization of granular media*, Arch. Rat. Mech. Anal., 179 (2006), pp. 217–263.
- [28] J.A. CARRILLO AND G. TOSCANI, *Exponential convergence toward equilibrium for homogeneous Fokker-Planck-type equations*, Math. Meth. Appl. Sci., 21 (1998), pp. 1269–1286.
- [29] J.A. CARRILLO AND G. TOSCANI, *Asymptotic L^1 -decay of solutions of the porous medium equation to self-similarity*, Indiana Univ. Math. J., 49 (2000), pp. 113–141.
- [30] J.A. CARRILLO AND G. TOSCANI, *Wasserstein metric and large-time asymptotics of nonlinear diffusion equations*, New Trends in Mathematical Physics, (In Honour of the Salvatore Rionero 70th Birthday), World Scientific, 2005.

- [31] J. DOLBEAULT AND B. PERTHAME, *Optimal critical mass in the two-dimensional Keller-Segel model in \mathbb{R}^2* , C. R. Math. Acad. Sci. Paris, 339 (2004), pp. 611–616.
- [32] L.C. EVANS, O. SAVIN, AND W. GANGBO, *Diffeomorphisms and nonlinear heat flows*, SIAM J. Math. Anal., 37 (2005), pp. 737–751.
- [33] F. FILBET, *A finite volume scheme for the Patlak-Keller-Segel chemotaxis model*, Numerisch. Math., 104 (2006), pp. 457–488.
- [34] F. GOLSE, *The mean-field limit for the dynamics of large particle systems*, Journées “Équations aux Dérivées Partielles”, Exp. No. IX, 47, Univ. Nantes, Nantes, 2003.
- [35] L. GOSSE AND G. TOSCANI, *Identification of asymptotic decay to self-similarity for one-dimensional filtration equations*, SIAM J. Numer. Anal., 43 (2006), pp. 2590–2606.
- [36] L. GOSSE AND G. TOSCANI, *Lagrangian numerical approximations to one-dimensional convolution-diffusion equations*, SIAM J. Sci. Comput., 28 (2006), pp. 1203–1227.
- [37] S. HAKER, A. TANNENBAUM, *Optimal Mass Transport and Image Registration*, Workshop on: Variational and Level Set Methods in Computer Vision, Proceedings. IEEE, (2001), pp. 29–36.
- [38] S. HAKER, L. ZHU, A. TANNENBAUM, AND S. ANGENENT, *Optimal Mass Transport for Registration and Warping*, International Journal on Computer Vision, 60 (2004), pp. 225–240.
- [39] R. JORDAN, D. KINDERLEHRER, AND F. OTTO, *The variational formulation of the Fokker-Planck equation*, SIAM J. Math. Anal., 29 (1998), pp. 1–17 (electronic).
- [40] E.F. KELLER AND L.A. SEGEL, *Initiation of slide mold aggregation viewed as an instability*, J. Theor. Biol., 26 (1970).
- [41] D. KINDERLEHRER AND N. WALKINGTON, *Approximation of Parabolic Equations Based Upon Wasserstein’s Variational Principle*, M2AN, 33 (1999), pp. 837–852.
- [42] H. LI AND G. TOSCANI, *Long-time asymptotics of kinetic models of granular flows*, Arch. Rat. Mech. Anal., 172 (2004), pp. 407–428.
- [43] F. LIU, S. JI AND G. LIAO, *An adaptive grid method and its application to steady Euler flow calculations*, SIAM J. Sci. Comput., 20 (1999), pp. 811–825.
- [44] R. J. MCCANN, *Existence and uniqueness of monotone measure-preserving maps*, Duke Math. J. 80, (1995), pp. 309–323.
- [45] R. J. MCCANN, *Polar factorization of maps on Riemannian manifolds*, Geom. Funct. Anal., 11 (2001) pp. 589–608.
- [46] R. J. MCCANN AND M. PUEL, *Constructing a relativistic heat flow by time transport steps*, preprint.
- [47] D. MORALE, V. CAPASSO AND K. OELSCHLÄGER, *An interacting particle system modelling aggregation behavior: from individuals to populations*, J. Math. Biol., 50 (2005), pp. 49–66.
- [48] A. OKUBO, S. LEVIN, *Diffusion and Ecological Problems: Modern Perspectives*, Springer, Berlin, 2002.
- [49] F. OTTO, *Doubly degenerate diffusion equations as steepest descent*, unpublished preprint (1996).
- [50] F. OTTO, *The geometry of dissipative evolution equations: the porous medium equation*, Comm. Partial Differential Equations, 26 (2001) pp. 101–174.
- [51] C.S. PATLAK, *Random walk with persistence and external bias*, Bull. Math. Biophys., 15 (1953), pp. 311–338.
- [52] G. PAPANICOLAOU, C. SULEM, P.L. SULEM, X. WANG, *Dynamic rescaling for tracking point singularities: application to nonlinear Schrödinger equation and related problems*, Singularities in fluids, plasmas and optics (Heraklion, 1992), NATO Adv. Sci. Inst. Ser. C Math. Phys. Sci., 404 (1993), pp. 265–279.
- [53] C.M. TOPAZ AND A.L. BERTOZZI, *Swarming patterns in a two-dimensional kinematic model for biological groups*, SIAM J. Appl. Math., 65 (2004), pp. 152–174.
- [54] C.M. TOPAZ, A.L. BERTOZZI, AND M.A. LEWIS, *A nonlocal continuum model for biological aggregation*, Bulletin of Mathematical Biology, 68(7), pp. 1601–1623, 2006.
- [55] G. TOSCANI, *One-dimensional kinetic models of granular flows*, RAIRO Modél. Math. Anal. Numér., 34, 6 (2000), pp. 1277–1291.
- [56] J.L. VÁZQUEZ, *The porous medium equation*, Oxford Mathematical Monographs, Oxford University Press, Oxford, 2007.
- [57] J. J. L. VELÁZQUEZ, *Point dynamics in a singular limit of the Keller-Segel model. I. Motion of the concentration regions*, SIAM J. Appl. Math., 64 (2004), pp. 1198–1223 (electronic).
- [58] J. J. L. VELÁZQUEZ, *Point dynamics in a singular limit of the Keller-Segel model. II. Formation of the concentration regions*, SIAM J. Appl. Math., 64 (2004), pp. 1224–1248.
- [59] C. VILLANI, *Topics in optimal transportation*, Graduate Studies in Mathematics Vol. 58, Amer. Math. Soc, Providence, 2003.